45th AIAA Aerospace Sciences Meeting and Exhibit
8 - 11 January 2007, Reno, Nevada

AIAA 2007-1130

Utilizing CFD-Based Exergy Calculations in the Design/Optimization of a Complete Aircraft System

Kehinde Alabi* and Foluso Ladeinde.†
Thaerocomp Technical Corp., P. O. Box 1527, Stony Brook, NY, 11790-0609

This paper reports on the use of CFD-based exergy calculation procedure in the multi-disciplinary design and optimization of a complete aircraft system. The procedure is a multi-level one which is based on physical decomposition of the overall system into various sub-systems and utilizes the iterative local/global optimization procedure for system level optimization to avoid the implicit nesting of optimization loops. The procedure thus allows each subsystem to be modeled to a level of detail desired at the subsystem level. Formulation of the CFD-based exergy calculation and results are presented, as is the procedure for both single point and multi-point optimization of the air-frame subsystem of the aircraft. Results from CFD-based modeling are further compared with those from traditional methods based on empirical formulation.

Nomenclature

C_p = pressure coefficient
f = friction factor
M_∞ = free stream Mach number
J = Jacobian of the coordinate transformation matrix
k = turbulence kinetic energy
Pr_T = turbulence Prandtl number
s = entropy generation
S_{ij} = "*ij*" component of the strain rate tensor
$\dot{S}_{gen}$ = entropy generation rate per unit volume
T_w = wall temperature
γ = ratio of specific heats
t = time
u, v, w = velocity components in the x, y, z Cartesian coordinate directions, respectively
u_τ = friction velocity
(x, y, z) = the Cartesian coordinate directions
y^+ = shortest distance to the nearest wall normalized by the friction velocity and fluid kinematic viscosity
α = angle of attack
μ_T, ν_T = turbulence dynamic and kinematic viscosities, respectively
ρ = fluid density
ε = turbulence kinetic energy dissipation rate
τ_{ij} = the "*ij*" component of the shear stress tensor
(ξ, η, ζ) = the curvilinear coordinate directions

I. INTRODUCTION

The design of a complete aircraft is a complicated undertaking consisting of several variables, and requiring the convergence of different technologies and experts from different disciplines. While many engineering research activities tend to focus on a specific aspect or detail of an engineering system, design/optimization research has a focus on the entire system as a unit, incorporating the complex interactions and requirements of the various smaller subsystems or components comprising the system. By this definition, design/optimization problems are quite complex. Traditionally,

* Research Engineer, Ph.D, AIAA Member.
† Director of Research, AIAA Life Member & Associate Fellow.

engineers have tackled this complex system design effort by using trade-off analysis, handbooks and specifications, and rule of thumb. With increasing computational power, attention has focused on the solution of design/optimization problem in an integrated manner. Initial solutions have been based on reduced models in which many of the subsystem or component details are represented by less complicated models. Less detail may lead to manageable problems but entails a loss of information which tends to make the result of such optimization questionable or of little use.

The overall objective of an aircraft design/optimization undertaking is to obtain an optimized or "best" system incorporating all the model details of the components of the system, as a single problem or in an integrated or single-level effort. Formulating and solving the synthesis/design, analysis/optimization problem for aerospace systems as a single-level problem is very difficult, if not impractical. The first reason is the huge size of such problems and the number of variables contained in such an analysis. Secondly, the tools for analyzing the different components and/or subsystems typically consist of disparate computer programs on different platforms making an integrated analysis extremely difficult. A third reason is the fact that most systems are designed by several different engineering units, sometimes at different geographical locations, and even sometimes from different organizations. Consequently, procedures that utilize a multi-level approach or utilize decomposition methods are more attractive.

Several decomposition methods have been used to break up the design problem into several levels including physical, disciplinary, conceptual, and time based decomposition.[1-4] Decomposing the problem into subsystems allows the modeling of each subsystem by different groups of engineers and at different locations. This also makes the scope of the problem more manageable.

Another issue faced during design optimization of aircraft systems is the issue of whether to design for a single design point or over an entire mission. Designs optimized for a single point in service are easier to formulate but do not guarantee an optimal vehicle over a mission range and/or over the life of the vehicle, nor does if consider variations in atmospheric conditions with different missions.

To address the single point/multi-design point, single/multi-level issue, particularly with respect to large-scale optimization, Munoz and von Spakovsky[5] and Rancruel and von Spakovsky[6,7] have, for example developed and successfully applied various decomposition procedures for the resolution of the large-scale synthesis/design optimization problem of a high performance aircraft system. The systems considered comprised of multiple subsystems including the airframe – aerodynamics, propulsion, fuel loop, environmental control, thermal management, electrical, hydraulic, oil loop, controls, expendable payload, and equipment group subsystems. The procedure developed in their work was extended in the current study.

The next question is how much detail from the components needs to be integrated at the system level. The answer to this question is usually constrained by computational resources. An advantage of multi-level approaches is that it permits varying levels of details or degrees of fidelity to be used in an integrated fashion. An analysis may be commenced with more approximate models at each level and refined as the analysis proceeds. However, a problem with multi-level optimization efforts is the nested optimization loops implied in the procedure. The iterative local-global optimization (ILGO) procedure[1,5-7] addresses this problem by removing the need to nest the optimization by using "shadow functions" or a gradient-type formulation based on the coupling functions at the system level. In the current paper, we examine procedures to alternatively utilize high-fidelity computational fluid dynamics (CFD) calculations to model the Air Frame subsystem of a modern commercial aircraft and compare the results with those utilizing a lumped parameter model. In addition, we demonstrate how the formulation fits with the iterative local global multi-level approach.

In the current study, the objective function is based on exergy destruction. Exergy is a measure of the maximum theoretical work that can be obtained from a system and unlike energy based objective function measures both energy as well as the quality of the energy in a system. Exergy combines balances of mass, energy, and entropy into a single balance of exergy. In addition, exergy-based analysis allows the designer to identify areas of high exergy destruction and consequently potential for design improvement.

II. Design/Optimization Analysis Procedures

The techniques for handling a multi-level design/optimization problem can be divided into three tasks shown in figure 1.

A. Decomposition

Physical decomposition divides the system along sub-system lines. In this sense, the system is composed of physically interacting subsystems each possessing a certain degree of autonomy but depending on other subsystems via a number of couplings or shared variables (Alexandrov & Kodiyalam, 1998).[2] For instance, the environmental control sub-system is distinct from the propulsion sub-system in that the physical components contained in each sub-system are distinct and separate but are coupled by several variables.[1,12,13,17,18] Disciplinary decomposition divides the system along the lines of different disciplines such as thermodynamic, economic, aerodynamic, etc. Conceptual decomposition breaks down the system according to the type of variables, for instance operational variables which vary in time and static ones. Time decomposition transforms or decomposes a dynamic problem into a series of quasi-stationary ones consisting of a series of stationary time segments.[17,18]

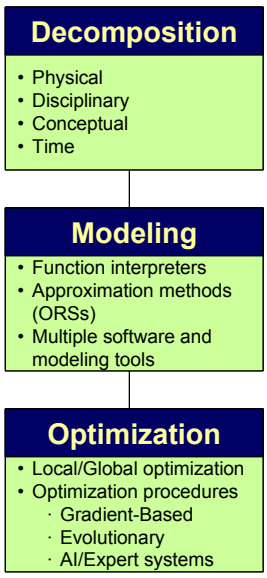

Figure 1. Parts of an applied MDO analysis

B. Modeling

Modeling of the various components and subsystems typically involves several engineering software from different providers. The greatest challenge in this step is usually the integration of the different software. Several levels can be identified in the multi-level modeling and optimization process:

Low Level Function Interpreters and Symbolic Language Programs

These are tools that allow an engineer to specify the equations and models comprising a component in mathematical form, aggregating these low level models into higher level models through additional mathematical expressions and functions. Technically, a complete system can be built using these tools. However, the procedure is quite difficult and prone to error at every level.

Aggregated Component Tools

This involves the use of prepackaged tools for specific models such as the use of an engine simulator for computing the thrust and weight of the propulsion system (e.g. Weight Analysis of Turbine Engines, WATE) or a heat exchanger program for the various heat exchangers in the sub-systems of the aircraft. Component tools are typically treated as a black box in the integration of the models into the complete system.

Approximation Tools

Response surfaces may be generated from experiments or measurements of a component or sub-system as a function of selected decision variables and used as the model in the multi-level optimization phase.

C. Optimization

Several tools have been used to optimize a complete system based on a multi-level optimization of the various subsystems. Available procedures include gradient-based methods that work well for subsystems with continuous variables but are prone to local optima. Procedures based on evolutionary algorithms and expert systems are more computationally intensive but are not prone to local optima and can be used for mixed integer problems. A combination of several optimization procedures is typically used for a complex problem – selecting the most fitting technique for each subsystem. However, the optimization within each subsystem is typically nested within the global optimization with the variation of each coupling variable or function connecting the subsystems.

D. The Iterative Local/Global Optimization Procedure

The iterative local/global optimization procedure[2,5-7,17,18] avoids the need for nested optimization by utilizing the gradient or response of each subsystem to the variation of the coupling functions.

Considering a system decomposed into two subsystems with variables, $\vec{x}_1, \vec{x}_2$, and the model equations:

$$\vec{H}_1(\vec{x}_1) = 0, \vec{H}_2(\vec{x}_2) = 0$$

and constraints

$$\vec{G}_1(\vec{x}_1) \le 0, \vec{G}_2(\vec{x}_2) \le 0$$

and objective function

$$F = F_1(x_1, u_{12}, u_{21}) + F_2(x_2, u_{12}, u_{21})$$

Assuming the coupling function u_{12}, u_{21} between the subsystems, the overall objective becomes:

Minimize

$$F = F_1(x_1, u_{12}, u_{21})$$

w.r.t. $\vec{x}_1$

$$\vec{H}_1(\vec{x}_1) = 0$$
$$\vec{G}_1(\vec{x}_1) \le 0$$

and

$$F = F_2(x_2, u_{12}, u_{21})$$

w.r.t. $\vec{x}_2$

$$\vec{H}_2(\vec{x}_2) = 0$$
$$\vec{G}_2(\vec{x}_2) \le 0$$

Assuming the resulting values for the optimum solutions are F_{1o}, and F_{2o}, then

$$F_1^* = F_{1o} + \frac{\partial F_1^*}{\partial u_{12}} \Delta u_{12} + \frac{\partial F_1^*}{\partial u_{21}} \Delta u_{21}$$
$$F_2^* = F_{2o} + \frac{\partial F_2^*}{\partial u_{12}} \Delta u_{12} + \frac{\partial F_2^*}{\partial u_{21}} \Delta u_{21}$$

Depending on the sign of the partial derivatives of the coupling functions, improved estimates of the coupling functions may be obtained from the above equations.

III. Formulation

The objective is to compute the exergy destruction rate of the Airframe subsystem aerodynamics (AFS-A) as a part of the overall exergy objective function. An option is to use lumped parameter models or to use CFD. Lumped parameter models are approximate relationships based on aggregate parameters, such as the wing thickness, span, and aspect ratio. Using CFD can provide more accurate results than the lumped models but require more time. In addition, lumped parameter models may not be applicable or exist for a specific aircraft configuration.

A. Lumped Parameter Estimates

For an uncambered wing, the lift-drag relationship may be expressed as:

$$C_D = K_1 C_L^2 + C_{D0}$$

The drag can be estimated as

Subsonic

$$C_{D0} = C_{D\min} = C_{fe} \frac{S_{wet}}{S_{ref}}$$

Supersonic

$$C_{D0} = C_{fe} \frac{S_{wet}}{S_{ref}} + C_{Dwave}$$

In addition, the lift factor, K_1, can be estimated by

Subsonic

$$K_1 = \frac{1}{AR \cdot e \cdot \pi}$$

Supersonic

$$K_1 = \frac{AR\left(M^2 - 1\right)}{4AR\sqrt{M^2 - 1}} - 2\cos\Lambda_{LE}$$

where AR is the wing aspect ratio, M is the Mach number, Λ_{LE} is the quarter chord sweep angle, e is the span efficiency factor, C_{fe} is the skin friction factor, and C_{Dwave} is the drag coefficient due to wave shocks.

The following expressions are often used to estimate the lift coefficient in the above expression:

Subsonic Lift Slope

$$C_L = \alpha C_{L\alpha}$$

where $C_{L\alpha}$ is the wing lift curve slope, and α is the angle of attack.

Where its value is not available, $C_{L\alpha}$ may further be estimated by

$$C_{L\alpha} = \frac{2AR\pi}{2 + \sqrt{4 + \frac{AR^2\beta^2}{\eta^2}\left(1 + \frac{\tan^2\Lambda_{\max t}}{\beta^2}\right)}}\left(\frac{S_{\exp}}{S_{ref}}\right)F$$

where

$$\beta^2 = 1 - M^2$$

$$\eta = \frac{C_{l\alpha}}{2\pi/\beta}$$

$$F = 1.07\left(1 + d/b\right)^2$$

In the above equations, $\Lambda_{\max t}$ is the sweep angle of the wing at the chord location where the airfoil is thickest, $C_{l\alpha}$ is the airfoil lift curve slope, S_{exp} is the exposed wing platform, F is the fuselage lift factor, which accounts for the lift due to interaction between the wing and the fuselage, d is the fuselage maximum equivalent diameter, and b is the wing span.

Supersonic Lift Slope

$$C_L = \alpha C_{L\alpha}$$

where $C_{L\alpha}$ may be estimated as

$$C_{L\alpha} = \frac{4}{\beta}$$

when $M > 1/\cos\Lambda_{LE}$

Estimating the Skin Friction Coefficient

The component build up method (Raymer, 2000)[22] can be used to estimate the subsonic parasitic drag from each component of the aircraft using a calculated flat-plate skin-friction drag coefficient, C_f, and a component form factor (FF) which accounts for the pressure drag due to viscous separation. The interference effects on the component drag are calculated as the factor Q. The subsonic parasitic drag is given by:

$$C_{D0} = \frac{\sum\left(C_f FFQS_{wet}\right)_c}{S_{ref}} + C_{DMISC} + C_{DL\&P} \quad (1)$$

where C_{DMISC} is the miscellaneous drag coefficient, which accounts for special features such as flaps, upsweep aft fuselage, base area, etc. $C_{DL\&P}$ is the contribution for leakage and protuberances. The subscript c indicates that those parameters are different for each component.

The flat-plate skin friction coefficient, C_f, depends on Reynolds number, Mach number, and skin roughness. The most important factor affecting skin-friction drag is whether or not the flow is laminar or turbulent. The expressions for skin-friction for a flat plate are shown below:

Laminar:

$$C_f = \frac{1.328}{\sqrt{\mathrm{Re}}}$$

Turbulent:

$$C_f = \frac{0.455}{\left(\log_{10}\mathrm{Re}\right)^{2.58}\left(1+0.144M^2\right)^{0.65}} \tag{2}$$

$$\mathrm{Re} = \rho U_\infty l / \mu$$

where l is the characteristic length and U_∞ is the speed of the aircraft.

The form factor can be estimated for each component as follows:

Wing, Tail, Strut, and Pylon:

$$FF = \left[1+\frac{0.6}{(x/c)_m}\left(\frac{t}{c}\right)+100\left(\frac{t}{c}\right)^4\right]\left[1.34M^{0.018}\left(\cos\Lambda_m\right)^{0.28}\right] \tag{3}$$

Fuselage and Smooth Canopy:

$$FF = \left[1+\frac{0.6}{f^3}+\frac{f}{400}\right] \tag{4}$$

Nacelle or any smooth External Store:

$$FF = 1+\left(\frac{0.35}{f}\right) \tag{5}$$

where $(x/c)_m$ is the chord-wise location at the airfoil maximum thickness point. Is the sweep angle at the maximum thickness line, and f is given by

$$f = \frac{l}{d} = \frac{l}{\sqrt{(4/\pi)A_{\max}}}$$

The component interference factor Q is used to account for increase in parasitic drag due to the mutual interference between components. Estimates for this quantity were obtained from Raymer (2000).[22]

Leaks and protuberances add drag and are difficult to predict by any method. Leakage drag is due to the tendency of an aircraft to "inhale" through holes and gaps in high pressure zones and "exhale" in low pressure zones. Protuberances include antennas, lights, fuel vents, actuators, etc. These quantities are ignored as they are not included in the CFD model to which the current estimates will be compared.

The supersonic parasitic drag is given by:

$$C_{D0} = \frac{\sum\left(C_f S_{wet}\right)_c}{S_{ref}} + C_{DMISC} + C_{DL\&P} + C_{Dwave} \tag{5}$$

where C_{Dwave} is the drag due to shocks and can be estimated as

$$C_{Dwave} = \frac{9\pi}{2S_{ref}}\left(\frac{A_{\max}}{l}\right) \tag{6}$$

which represents the minimum possible wave drag for any closed-body with the same length and volume – the "Sears-Haack" body. For a specific aircraft body, the Sears-Haack body drag can be modified by

$$C_{Dwave} = E_{WD}\left[1 - 0.386(M-1.2)^{0.57}\left(1 - \frac{\pi\Lambda_{LE}^{0.77}}{100}\right)\right]C_{Dwave\_S.Q.} \tag{7}$$

Exergy Calculation

The exergy destruction rate may be computed from the overall parasitic drag

$$Ex_{DES} = \frac{TD_{parasitic}V}{T_0} \tag{8}$$

where T is the average temperature of the aircraft, $D_{parasitic}$ is the total parasitic drag force, V is the speed of the aircraft, and T_0 is the reference temperature, typically taken as the "sea level" temperature. The values for the required variables are shown in table 1.

Table 1. Variables for the AFS-A Empirical Model

Component	Variable		Initial Value/ Constraints
Wing	b/L	Wing span	7.5
	Λ_{LE}	Sweep angle	40^o
	AR	Aspect ratio	4.98
	t/c	Thickness ratio	0.2
	x/c	Thickest point	0.24
	Λ_m	Sweep angle at maximum thickness	10^o
	S_{wet}/S_{ref}	Flapped area to reference area	6.49308
	S_{ref}	Reference area (L^2)	69.324
Fuselage	l/L	Fuselage length	8.2
	d/L	Fuselage maximum diameter	0.76
	S_{ref} (m^2)	Reference area (L^2)	69.324

Based on the above equations and value, the friction and form factor for the components of the aircraft are:

Wing

C_f = 0.0033486, FF = 2.2075

Fuselage:

C_f = 0.00351128, FF = 1.02745

C_D = 0.0806.

The drag was calculated as 293,702.53N and the total exergy destruction rate as 8.69 x 10^7W.

B. The CFD Procedure

The CFD equations are those of the compressible Navier-Stokes equations.

$$\frac{\partial Q}{\partial t} + \frac{\partial(F - F_v)}{\partial \xi} + \frac{\partial(G - G_v)}{\partial \eta} + \frac{\partial(H - H_v)}{\partial \zeta} = 0, \tag{9}$$

where Q is the vector of solution variables, and F, G, and H are the Euler fluxes:

$$Q=\frac{1}{J}\begin{bmatrix}\rho\\ \rho u\\ \rho v\\ \rho w\\ E\end{bmatrix},\quad F=\frac{1}{J}\begin{bmatrix}\rho U\\ \rho uU+\xi_x p\\ \rho vU+\xi_y p\\ \rho wU+\xi_z p\\ (E+p)U\end{bmatrix},\quad G=\frac{1}{J}\begin{bmatrix}\rho V\\ \rho uV+\eta_x p\\ \rho vV+\eta_y p\\ \rho wV+\eta_z p\\ (E+p)V\end{bmatrix},\quad H=\frac{1}{J}\begin{bmatrix}\rho W\\ \rho uW+\zeta_x p\\ \rho vW+\zeta_y p\\ \rho wW+\zeta_z p\\ (E+p)W\end{bmatrix}, \tag{10}$$

and (U, V, W) are the contravariant velocity components defined as

$$U=\xi_x u+\xi_y v+\xi_z w,\qquad V=\eta_x u+\eta_y v+\eta_z w,\qquad W=\zeta_x u+\zeta_y v+\zeta_z w\,.$$

In the above equations, (u,v,w) are the velocity components in the Cartesian coordinate directions (x,y,z), ρ is the density, and p is the pressure. E is the total energy, which can be written as

$$E=\frac{p}{(\gamma-1)}+\rho\frac{u^2+v^2+w^2}{2}\,.$$

The viscous terms in Eq. (1) are

$$F_v=\frac{1}{J}\begin{bmatrix}0\\ \tau_{xx}\xi_x+\tau_{yx}\xi_y+\tau_{zx}\xi_z\\ \tau_{xy}\xi_x+\tau_{yy}\xi_y+\tau_{zy}\xi_z\\ \tau_{xz}\xi_x+\tau_{yz}\xi_y+\tau_{zz}\xi_z\\ (u\tau_{xx}+v\tau_{xy}+w\tau_{xz}+q_x)\xi_x+(u\tau_{yx}+v\tau_{yy}+w\tau_{yz}+q_y)\xi_y+(u\tau_{zx}+v\tau_{zy}+w\tau_{zz}+q_z)\xi_z\end{bmatrix},$$

$$G_v=\frac{1}{J}\begin{bmatrix}0\\ \tau_{xx}\eta_x+\tau_{yx}\eta_y+\tau_{zx}\eta_z\\ \tau_{xy}\eta_x+\tau_{yy}\eta_y+\tau_{zy}\eta_z\\ \tau_{xz}\eta_x+\tau_{yz}\eta_y+\tau_{zz}\eta_z\\ (u\tau_{xx}+v\tau_{xy}+w\tau_{xz}+q_x)\eta_x+(u\tau_{yx}+v\tau_{yy}+w\tau_{yz}+q_y)\eta_y+(u\tau_{zx}+v\tau_{zy}+w\tau_{zz}+q_z)\eta_z\end{bmatrix},$$

$$H_v=\frac{1}{J}\begin{bmatrix}0\\ \tau_{xx}\zeta_x+\tau_{yx}\zeta_y+\tau_{zx}\zeta_z\\ \tau_{xy}\zeta_x+\tau_{yy}\zeta_y+\tau_{zy}\zeta_z\\ \tau_{xz}\zeta_x+\tau_{yz}\zeta_y+\tau_{zz}\zeta_z\\ (u\tau_{xx}+v\tau_{xy}+w\tau_{xz}+q_x)\zeta_x+(u\tau_{yx}+v\tau_{yy}+w\tau_{yz}+q_y)\zeta_y+(u\tau_{zx}+v\tau_{zy}+w\tau_{zz}+q_z)\zeta_z\end{bmatrix},$$

where

$$\tau_{ij}=\frac{1}{\mathrm{Re}}\left[\left(\frac{\partial u_i}{\partial x_j}+\frac{\partial u_j}{\partial x_i}\right)-\frac{2}{3}\delta_{ij}\frac{\partial u_k}{\partial x_k}\right],\qquad q_i=\frac{1}{(\gamma-1)M^2\,\mathrm{Re}\,\mathrm{Pr}}\frac{\partial T}{\partial x_i}.$$

By using the implicit, approximately-factored finite-difference algorithm of Beam-Warming and employing a Newton-like sub-iteration, we have the following algorithm:

$$\left[J^{-1^{p+1}}+\phi^i\Delta t_s\delta_\xi\left(\frac{\partial\hat{F}^p}{\partial U}-\frac{1}{\mathrm{Re}}\frac{\partial\hat{F}_v^p}{\partial U}\right)\right]J^{p+1}\times\left[J^{-1^{p+1}}+\phi^i\Delta t_s\delta_\eta\left(\frac{\partial\hat{G}^p}{\partial U}-\frac{1}{\mathrm{Re}}\frac{\partial\hat{G}_v^p}{\partial U}\right)\right]J^{p+1}\times$$

$$\left[J^{-1^{p+1}}+\phi^i\Delta t_s\delta_\zeta\left(\frac{\partial\hat{H}^p}{\partial U}-\frac{1}{\mathrm{Re}}\frac{\partial\hat{H}_v^p}{\partial U}\right)\right]\Delta U$$

$$=-\phi^i\Delta t_s\left[J^{-1^{p+1}}\frac{(1+\phi)U^p-(1+2\phi)U^n+\phi U^{n-1}}{\Delta t}-U^p\left(\left(\frac{\xi_t}{J}\right)_\xi+\left(\frac{\eta_t}{J}\right)_\eta+\left(\frac{\zeta_t}{J}\right)_\zeta\right)\right]$$

$$-\phi^i\Delta t_s\left[\delta_\xi\left(\hat{F}^p-\frac{1}{\mathrm{Re}}\hat{F}_v^p\right)+\delta_\eta\left(\hat{G}^p-\frac{1}{\mathrm{Re}}\hat{G}_v^p\right)+\delta_\zeta\left(\hat{H}^p-\frac{1}{\mathrm{Re}}\hat{H}_v^p\right)\right],$$

where

$$\phi^i=\frac{1}{1+\phi},\Delta U=U^{p+1}-U^p.$$

and superscripts "p" and "n" denote the sub-iteration steps and the outer-loop time steps, respectively. In the above equations, (ξ, η, ς) are the curvilinear coordinate directions and Δt_s is the time step for the sub-iterations. Either a first or second-order temporal accuracy can be specified in the above iterative procedure by selecting $\phi=0$ or $\phi=1/2$. For $p=1$, $U^p=U^n$ and $U^{n+1}=U^p$ at convergence in *p*.

For high-order differencing of flow fields with shock waves, the weighted essentially non-oscillatory (WENO) procedure[24] is used, which can be summarized as follows, if we consider the ξ direction in Eq. (5) as an example:

$$\left.\frac{\partial\hat{F}}{\partial\xi}\right|_i=\frac{1}{\Delta\xi}\left\{\left[\tilde{R}_{Roe}\cdot\left(\tilde{R}_{Roe}^{-1}\cdot\hat{F}\right)\right]_{i+1/2}-\left[\tilde{R}_{Roe}\cdot\left(\tilde{R}_{Roe}^{-1}\cdot\hat{F}\right)\right]_{i-1/2}\right\},$$

where

$$\hat{F}_{i\pm1/2}=\frac{1}{2}\left[\hat{F}\pm\alpha\cdot\hat{U}\right]_{i+1/2},\quad\alpha=\max_u\left|\hat{F}'(u)\right|,$$

and

$$\hat{F}_{i+1/2}^{+}=\sum_{r=0}^{k-1}\omega_r\hat{F}_{i+1/2}^{(r)+},\quad\hat{F}_{i+1/2}^{-}=\sum_{r=0}^{k-1}\tilde{\omega}_r\hat{F}_{c,i+1/2}^{(r)-},\quad\hat{F}_{i+1/2}^{(r)}=\sum_{m=0}^{k-1}c_{rm}\hat{F}_{i-r+m},$$

$$\omega_r=\frac{\alpha_r}{\sum_{s=0}^{k-1}\alpha_s},\alpha_\gamma=\frac{d_r}{(\varepsilon+\beta_r)},\quad r=0,\ldots,k-1,$$

with ω_r as the normalized weights, $\overline{\omega}_r=\overline{\omega}_r(\omega_r)$ and d_γ are constants, ε is a robustness factor that prevents the occurrence of a zero denominator, while β_γ is a smoothness indicator, which is related to the undivided difference. The positive sign indicates upwind, while negative implies downwind. We set $\varepsilon\approx10^{-14}$ and use spectral radius from coupled equation systems to compute the value of α, as opposed to a component-wise procedure to determine this parameter. Note that c_{rm} are coefficients of Lagrange interpolation formula.[24]

C. CFD Entropy Calculation

The procedure for calculating the entropy is derived formulations based on the Onsager relations.[9] This relation is quasi-steady:

$$\dot{S}_{gen}=\frac{1}{T}\tau_{ij}\frac{\partial u_i}{\partial x_j}-\frac{q_k}{T^2}\frac{\partial T}{\partial x_k},\tag{11}$$

where the term on the left-hand side represents the entropy generation per unit volume. The first term on the right represents irreversibilities related to the degradation of mechanical energy into internal energy[25,26] while the second term represents irreversiblities related to heat transfer across finite temperature differences.

For the present studies, we have used a model based on eddy viscosity to calculate the average entropy generation per unit volume:

$$\bar{\dot{S}}_{gen} = \frac{1}{\bar{T}} \bar{\tau}_{ij} \frac{\partial \bar{u}_i}{\partial x_j} - \frac{\bar{q}_k}{\bar{T}^2} \frac{\partial \bar{T}}{\partial x_k}, \tag{12}$$

where eddy viscosity-type assumptions are made:

$$\bar{\tau}_{ij} = (\mu + \mu_T)\left(\frac{\partial \bar{u}_i}{\partial x_j} + \frac{\partial \bar{u}_j}{\partial x_i} - \frac{2}{3} \frac{\partial \bar{u}_k}{\partial x_k} \delta_{ij} \right),$$

and

$$\bar{q}_k = -\left(\frac{\mu}{\mathrm{Pr}} + \frac{\mu_T}{\mathrm{Pr}_T} \right) \frac{\partial \bar{T}}{\partial x_k}.$$

The average entropy generation rate can be expressed in non-dimensional form as follows:

$$\begin{aligned} \bar{\dot{S}}_{gen} = \frac{1}{\mathrm{Re}} \frac{\mu + \mu_T}{\bar{T}} \Bigg\{ & 2\left(\frac{\partial \bar{u}}{\partial x} \right)^2 + 2\left(\frac{\partial \bar{v}}{\partial y} \right)^2 + 2\left(\frac{\partial \bar{w}}{\partial z} \right)^2 - \frac{2}{3}\left(\frac{\partial \bar{u}}{\partial x} + \frac{\partial \bar{v}}{\partial y} + \frac{\partial \bar{w}}{\partial z} \right)^2 + \\ & \left(\frac{\partial \bar{u}}{\partial y} + \frac{\partial \bar{v}}{\partial x} \right)^2 + \left(\frac{\partial \bar{u}}{\partial z} + \frac{\partial \bar{w}}{\partial x} \right)^2 + \left(\frac{\partial \bar{w}}{\partial y} + \frac{\partial \bar{v}}{\partial z} \right)^2 \Bigg\} \\ & + \frac{1}{(\gamma - 1) M_\infty^2 \, \mathrm{Re}\, \mathrm{Pr}} \frac{\mu / \mathrm{Pr} + \mu_T / \mathrm{Pr}_T}{\bar{T}^2} \left\{ \left(\frac{\partial \bar{T}}{\partial x} \right)^2 + \left(\frac{\partial \bar{T}}{\partial y} \right)^2 + \left(\frac{\partial \bar{T}}{\partial z} \right)^2 \right\}, \end{aligned} \tag{13}$$

where, for the curvilinear coordinate system used, we have

$$\frac{\partial u_i}{\partial x_j} = \frac{\partial u_i}{\partial \xi} \xi_{x_j} + \frac{\partial u_i}{\partial \eta} \eta_{x_j} + \frac{\partial u_i}{\partial \varsigma} \varsigma_{x_j},$$

$$\frac{\partial T}{\partial x_j} = \frac{\partial T}{\partial \xi} \xi_{x_j} + \frac{\partial T}{\partial \eta} \eta_{x_j} + \frac{\partial T}{\partial \varsigma} \varsigma_{x_j}.$$

Note that integration over volume of the entropy per unit volume is required in order to obtain the total entropy generation in the domain. Also note that the above formulation allows the rate of entropy generation to be computed as a derived (post-processed) quantity.

The exergy destruction rate in the control volume represented by the CFD domain may be expressed as:

$$\frac{dE_x}{dt} = \sum_{k=0}^{\kappa} \left(1 - \frac{T_0}{T_k} \right) \dot{Q}_k - \dot{W}_S - T_0 \dot{S}_{irr} + \sum_{j=1}^{IN} \dot{m}_j (e_x)_j - \sum_{j=1}^{OUT} \dot{m}_j (e_x)_j \tag{14}$$

where

$$e_x = h - T_0 s - \mu_0 + \frac{\xi^2}{2} + gz \tag{15}$$

$$E_x = E - T_0 S + P_0 V - \sum_{l=1}^{n} \mu_{l_0} m_l \tag{16}$$

where h, s, μ, m, and T_0 are the specific enthalpy, entropy, chemical potential, constituent mass, and "dead state" temperature respectively, while ξ and z are the velocity and elevation of the bulk flows entering and exiting the control volume.

For steady state

$$0 = \dot{E}_x^Q - \dot{W} - \dot{E}x_{DES} + \dot{E}x - \dot{E}x_e \tag{17}$$

From the Guoy-Stodola relation, the rate of irreversibilities occurring in a process is directly proportional via the "dead state" temperature to the rate of entropy generation:

$$\dot{I} = T_0 \dot{S}_{irr} = \dot{E}x_{DES} \tag{18}$$

where, of course, the rate of exergy destruction which occurs in the process is equal to the rate of irreversibilities. For the AFSA, the only contribution to exergy destruction is the entropy destruction as well as heat loss from the airframe:

$$\dot{E}x = \sum_{k=0}^{\kappa}\left(1-\frac{T_0}{T_k}\right)\dot{Q}_k + T_0\dot{S}_{irr} \tag{19}$$

Observations have shown that the contributions to the entropy generation rate in Eq. (13) show very steep gradients close to a wall and numerical simulations are far more effective with wall functions for the production terms.[26,28] This is particularly important for simulations with large values of y^+ (necessary when it is computationally impractical to resolve the flow at the wall for large calculations). The high Reynolds number k–ε model employs wall functions in place of fine resolutions at the wall. It has been used for turbulent entropy calculations.[21] The details of the model are presented below.

D. Turbulence Viscosity Model

The turbulent shear stress is approximated in the eddy viscosity form:

$$\tilde{\tau}'_{ij} = 2\tilde{\mu}_T\left[\tilde{S}_{ij} - \frac{1}{3}\frac{\partial\tilde{u}_k}{\partial x_k}\delta_{ij}\right] - \frac{2}{3}\tilde{\rho}k\delta_{ij},$$

where $\tilde{S}_{ij} = \frac{1}{2}\left(\frac{\partial\tilde{u}_i}{\partial x_j} + \frac{\partial\tilde{u}_j}{\partial x_i}\right)$ is the mean strain rate, $k = \frac{1}{2}\left(u'^2 + v'^2 + w'^2\right)$ is the turbulent kinetic energy, $\mu_t = C_\mu f_\mu \frac{\rho k^2}{\varepsilon}$ is the eddy viscosity, and ε is the dissipation rate of k. The following equations are solved for k and ε:

$$\frac{\partial k}{\partial t} + \tilde{u}_j\frac{\partial k}{\partial x_j} - \frac{1}{\rho}\frac{\partial}{\partial x_j}\left(\left(\tilde{\mu} + \frac{\tilde{\mu}_t}{\rho_k}\right)\frac{\partial k}{\partial x_j}\right) = P - \varepsilon$$

$$\frac{\partial \varepsilon}{\partial t} + \tilde{u}_j\frac{\partial \varepsilon}{\partial x_j} - \frac{1}{\rho}\frac{\partial}{\partial x_j}\left(\left(\tilde{\mu} + \frac{\tilde{\mu}_t}{\rho_\varepsilon}\right)\frac{\partial \varepsilon}{\partial x_j}\right) = \frac{C_1}{\rho}\frac{\varepsilon}{k}P - \frac{C_2\varepsilon^2}{k}.$$

The constants in the above equations are $C_\mu = 0.09$, $\rho_\kappa = 1.0$, $\rho_\varepsilon = 1.3$, $C_1 = 1.44$, $C_2 = 1.92$ and $P = \tilde{\tau}_{ij}\tilde{S}_{ij}$ is the turbulent production. For boundary conditions, a two layer "law of the wall" was used to impose the k and ε values at the first point (on the wall). A wall function was also used in the viscous sublayer. Details of the formulation can be found in the work of Steffen.[29]

IV. Calculation of Flow over Boeing 747-200 Commercial Aircraft

The entropy production associated with the flow over a Boeing 747-200 commercial aircraft was calculated, as a way of generating exergy-based design data for the AFS-A subsystem of an integrated aircraft design/synthesis analysis. The following conditions were used: $M_\infty = 0.855$, $\alpha = 3.05^o$, reference area = 5500 sq ft (792,000 sq in), moment center = (1339.91, 0.0, 191.87) in., moment reference length = 327.8 in., and Re = 10680 per in. The spatial dimensions have been normalized with the moment reference length, leading to a reference Reynolds number, $Re = 3.5\times10^6$. Both Euler and Navier-Stokes calculations were carried out using high-order discretization. The computational grids contained nine blocks with the following grid points: fuselage 138 x 70 x 30 = 416,000, nose cone 31 x 20 x 30 = 18,600, tail cap $(31\times20\times30 = 18{,}600)$, wing base 129 x 38 x 30 = 147,060, wing mid section 50 x 129 x 29 = 187,050, wing tip (top) 77 x 41 x 28 = 81,508, wing tip (bottom) 77 x 41 x 28 = 81,508, wing patch 71 x 71 x 71 = 357,911, and far-field grid 73 x 39 x 48 = 136,656. This yields a total number of grid points of 1,444,993. The first grid at the wall is located approximately at $\Delta y = 1 \times 10^{-4}$ which corresponds to a $y^+ \approx 80$. The grid used for the calculations is shown in Fig. 2 and described below.

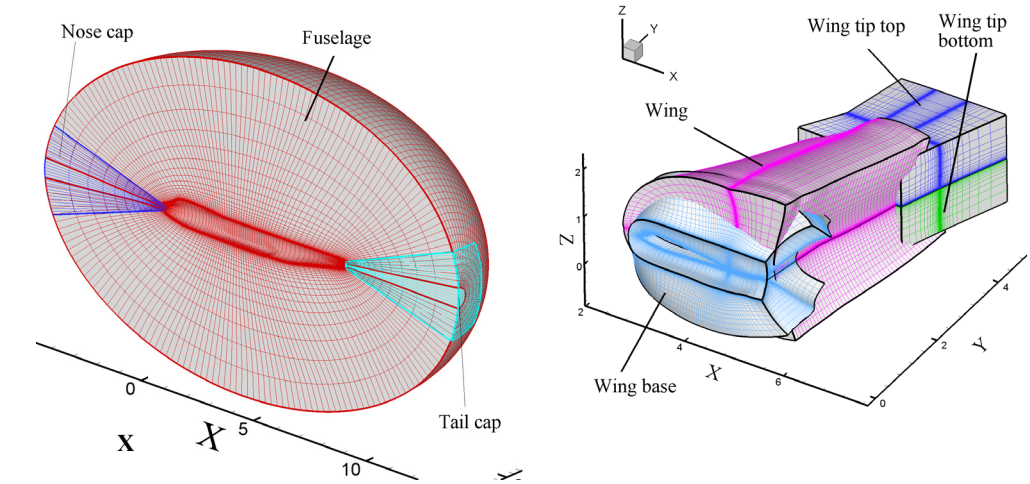

Figure 2. Mesh used for the computation of flow around the B747-200.

A. The B747-200 overset grid system

The fuselage surface is modeled using three overset blocks shown in Fig. 2(a). Block 2 (fuselage) spans most of the fuselage length in the physical x-direction. Blocks 3 and 4 are designed to cover the nose and tail surfaces of the fuselage. The later blocks are necessary to avert the computational singularities near the two poles.

Figure 2(b) shows an ensemble view of the computational grids, Blocks 5 through 8, around the wing. Block 5 (wing base) is a C-H type grid designed to connect the wing and fuselage surfaces. Block 6 (wing) is a C-type grid and extends over most of the wing span. Blocks 7 and 8 (wing tip top and bottom) consist of the H-H topology. The computational blocks around the wing exhibit enhanced grid density near the wing trailing edge and near the wing tip. For all computational blocks near solid walls (Blocks 2 through 8) the normalized grid space value at the wall is $\Delta = 1\times10^{-4}$.

A far-field box-shaped grid (not shown in Fig. 1) is designed to connect the computational blocks near the fuselage and the wing with far field conditions. For Block 1, the grids are clustered near the fuselage and wing blocks in all computational directions.

Details of the calculation and some of the difficulties encountered in performing the simulations are presented in Ladeinde et. al.[21] The results are discussed below.

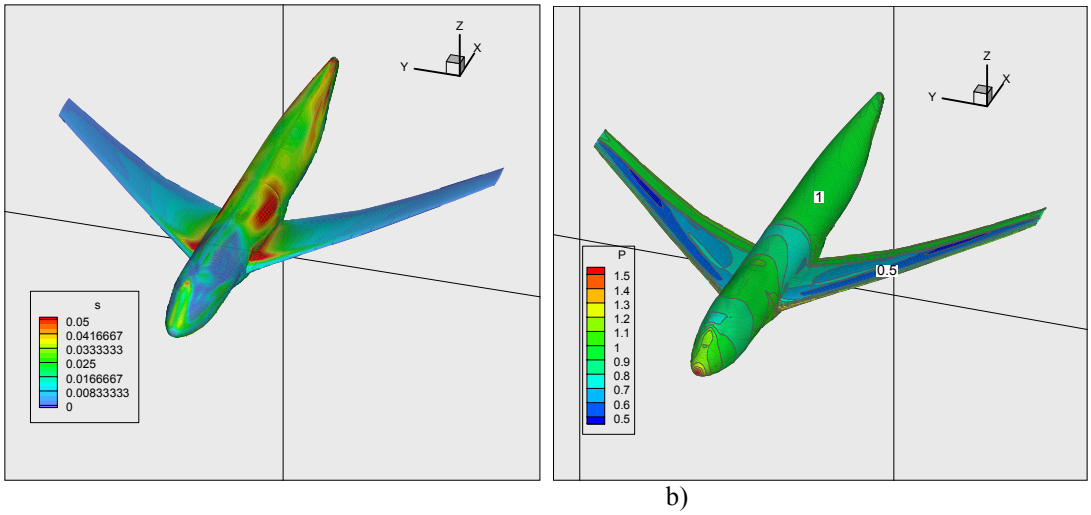

Figure 3. Contours of (a) entropy generation and (b) pressure around the B747-200 aircraft

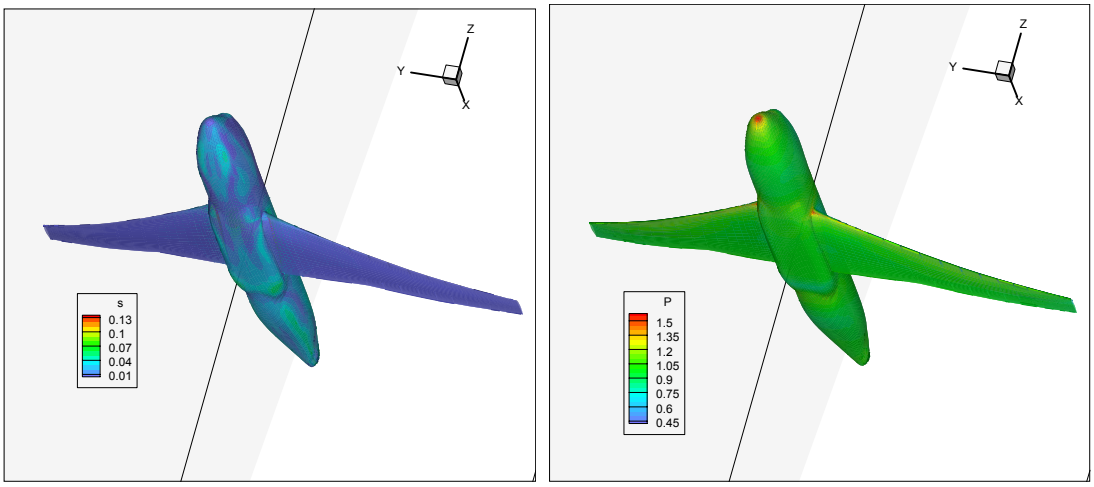

a) b)

Figure 4. Contours of (a) entropy generation and (b) pressure around the bottom of the B747-200 aircraft

Figure 3 shows the entropy and pressure contours at the top of the fuselage and the suction side of the wing while Fig. 4 shows the analogous plots at the bottom of the fuselage and the pressure side of the wings, respectively. From these figures, it can be noted that much of the entropy at the surface is generated on the top part of the plane, in the nose region and in the tip of the wing where the velocity gradients are maximum. In addition, high entropy generation can be found on the fuselage just above the wings and on the wings close to the junction where the wings and fuselage meet. On the bottom surface, most of the entropy is generated along the most curved surfaces where the velocity gradients are a maximum.

The total exergy destruction over a range of angle of attack is presented in the table below. The results show some relationship between the exergy values obtained via CFD and those obtained from empirical relationships. In particular, both calculations show a similar trend with increasing angle of attack.

Table 2. Comparison of Exergy and Aerodynamic Calculations Obtained via CFD and Empirical Relations

CFD

α	**0**	**1.05**	**2.05**	**3.05**
$T_0 S$	463.660	563.227	593.178	656.211
EX_Q	113.521	100.028	64.307	118.569
Ex	350.140	463.198	528.871	537.642
C_L	0.090	0.201	0.410	0.615
C_D	0.018	0.020	0.028	0.040
C_M	-0.026	-0.023	-0.025	-0.022
C_F	0.351	0.385	0.401	0.420
Drag	3.01E+05	3.30E+05	3.51E+05	3.76E+05
Ex(W)	8.92E+07	9.78E+07	1.04E+08	1.11E+08

Empirical Relations

α	**0**	**1.05**	**2.05**	**3.05**
C_L	0	0.226	0.441	0.657
$K_1 C_L$	0	0.018	0.035	0.052
Drag	2.94E+05	3.08E+05	3.22E+05	3.36E+05
Ex(W)	8.69E+07	9.13E+07	9.54E+07	9.96E+07

V. Conclusions

In the current paper, the feasibility of utilizing CFD calculations to model the AFS-A as part of a multi-disciplinary design optimization of a complete aircraft was demonstrated. The procedure is based on a multi-level decomposition and optimization of the various physical subsystems of the aircraft. System level optimization is obtained based on the iterative local/global optimization procedure which avoids the need for nested optimization by utilizing the gradient or

response of each subsystem to the variation of the coupling functions. In the procedure, the amount of model detail can be determined at the subsystem level. Using exergy as the objective function, calculations were presented to compare empirical models of the airframe subsystem to CFD models.

Acknowledgments

This work was funded by the United States Air Force under Contract FA8650-05-C-3521 via the Phase II SBIR program, with Dr. David Moorhouse as Technical Monitor. The authors are very grateful to the Air Force for giving Thaerocomp the opportunity to develop innovative research tools.

References

[1]Munoz, J. R.,, 2002, "A Decomposition Strategy Based on Thermoeconomic Isolation Applied to the Optimal Synthesis/Design and Operation of an Advanced Fighter Aircraft System," M..S. thesis, Advisor: M. R. von Spakovsky, Mechanical Engineering Dept., Virginia Polytechnic University, Blacksburg, VA February 2002.

[2]Alexandrov, N. M., Kodiyalam, S., 1998, "Initial Results of an MDO Method Evaluation Study," AIAA Paper: AIAA-98-4884.

[3]Le, A., Gray, K., Baker, M. L., 2003, "Building the Aerodynamics Module for the Integrated Hypersonic Aeromechanics Tool," AIAA Paper.

[4]Alabi, K., Ladeinde, F., von Spakovsky, M.R., Moorhouse, D., Camberos, J., "Assessing CFD Modeling of Entropy Generation for the Air Frame Subsystem in an Integrated Aircraft Design/Synthesis Procedure," AIAA Aerospace Sciences Meeting and Exhibit, Reno, NV, Jan 2006.

[5]Munoz, J. R., von Spakovsky, M. R., 2001, "The Application of Decomposition to the Large Scale Synthesis/Design Optimization of Aircraft Energy Systems," International Journal of Applied Thermodynamics, June, Vol. 4, No. 2.

[6]Brewer, K. M., 2005, "Exergy Methods for Mission-Level Analysis and Optimizatio of Generic Hypersonic Vehicle Concepts," M.S. thesis, Advisor: M. R. von Spakovsky, Mechanical Engineering Dept., Virginia Polytechnic University, Blacksburg, VA September 2005.

[7]Butt, J., 2005, "Exergy Analysis and Optimization Applied to an Aircraft System with Wing Morphing," M.S. thesis, Advisor: M. R. con Spakovsky, Mechanical Engineering Dept., Virginia Polytechnic University, Blacksburg, VA September 2005.

[8]Figliolla, R.S. and Tipton, R., 2000, "An Exergy-Based Methodology for Decision-Based Design of Integrated Aircraft Thermal Systems," Paper No. 00WAC-92. Society of Automotive Engineers.

[9]Iandoli, C. L. and Sciubba, E., 2000, "Entropy Generation Maps of a Low-Specific Speed Radial Compressor Rotor," ASME MECE, Advance Energy Systems Division, AES-Vol. 40.

[10]Markell, K., 2005, "Exergy Methods for the Generic Analysis and Optimization of Hypersonic Vehicle Concepts," M..S. thesis, Advisor: M. R. von Spakovsky, Mechanical Engineering Dept., Virginia Polytechnic University, Blacksburg, VA February 2005.

[11]Moorhouse, D. J, Hoke, C. M., Prendergast, J. P., 2002, "Thermal Analysis of a Hypersonic Inlet Flow with Exergy-Based Design Methods," International Journal of Applied Thermodynamics, ICAT, Istanbul Turkey, Vol. 5, No. 4.

[12]Munoz, J. R., von Spakovsky, M. R., 2001, "The Application of Decomposition to the Large Scale Synthesis/Design Optimization of Aircraft Energy Systems," International Journal of Applied Thermodynamics, June, Vol. 4, No. 2.

[13]Munoz, J. R., von Spakovsky, M. R., 2001, "A Decomposition Approach for the Large Scale Synthesis/Design Optimization of Highly Coupled, Highly Dynamic Energy Systems," International Journal of Applied Thermodynamics, June, Vol. 4, No. 2.

[14]Natalini, G. and Sciubba, E., 1999, "Minimization of the Local Rates of Entropy Production in the Design of Air-Cooled Gas Turbine Blades," Journal of Engineering for Gas Turbines and Power, Vol. 121, No. 3.

[15]Naterer, G., and Camberos, J. A., 2003. Jounral of Thermoophysics and Heat Transfer, 17(3), pp 360-371.

[16]Periannan, V., 2005, "Investigation of the Efects of Different Objective Functions/Figures of Merit on the Analysis and Optimization of High Performance Aircraft System Synthesis/Design," M..S. thesis, Advisor: M. R. von Spakovsky, Mechanical Engineering Dept., Virginia Polytechnic University, Blacksburg, VA February 2005.

[17]Rancruel, D. F., von Spakovsky, M. R., 2004, "Use of a Unique Decomposition Strategy for the Optimal Synthesis/Design and Operation of an Advanced Fighter Aircraft System," 10th AIAA/ISSMO Multi-disciplinary Analysis and Optimization Conference, Aug 30 – Sept 1, Albany New York.

[18]Rancruel, D. F., von Spakovsky, M. R., 2004, "Decomposition with Thermodynamic Isolation Applied to the Optimal Synthesis/Design of an Advanced Fighter Aircraft System," 10th AIAA/ISSMO Multi-disciplinary Analysis and Optimization Conference, Aug 30 – Sept 1, Albany New York.

[19]Riggins, D. 2003, "The Thermodynamic Continuum of Jet Engine Performance: The Principle of Lost Work due to Irreversibility in Aerospace Systems," International Journal of Thermodynamics, Vol. 6, No. 3.

[20]Roth, B. and Mavris, D., 2000, "A Method for Propulsion Technology Impact Evaluation via Thermodynamic Work Potential," AIAA Paper 20000-4854, September 2000.

[21]Ladeinde, F., Alabi, K., Safta, S., Cai, X., Johnson, F., 2006, "The First High-Order CFD Simulation of Aircraft: Challenges and Opportunities," AIAA Paper 2006-1526.

[22]Raymer, D.P., 1999, Aircraft Design: A Conceptual Approach.

[23]Adeyinka, O. B. and Naterer, G. F., "Modeling of Entropy Production in Turbulent Flows" J. Fluid Eng. Vol. 126, 2004.pp. 893-899.

[24]Harten, A., Engquist, B., Osher, S. and Chakravarthy, S. 1987. Uniformly high order essentially non-oscillatory schemes, III, , *J. Comp. Phys*. 71, pp. 231-303.

[25]Kramer-Bevan, J. S., "A tool for Analysis of Fluid Flow Losses" M.Sc Thesis, University of Waterloo, Canada,1992,.

[26]Bejan, A., "Entropy Generation Minimization: The Method of Thermodynamic Optimization of Finite-Time Systems and Finite-Time Processes", CRC Press. New York 1996.

[27]Moore, J., and Moore, J. G., 1983. "Entropy Production Rates from Viscous Flow Calculations, Part I. A Turbulent Boundary Layer Flow," ASME Paper 83-GT-70, ASME Gas Turbine Conference, Phoenix, AZ.

[28]F. Kock, H. Herwig: Local Entropy Production in Turbulent Shear Flows: A High Reynolds Number Model with Wall functions, erscheint in: Int. J. Heat Mass Transfer, 2004.

[29]Steffen, C. J., "A Critical Comparison of Several Low Reynolds Number k-ε Turbulence Models for Flow Over a Backward-Facing Step", NASA Technical Memorandum 106173. AIAA-93-1927.